
Article:
White, Robin J., Shuttleworth, Peter S., Budarin, Vitaliy L. et al. (3 more authors) (2016) An Interesting Class of Porous Polymer-Revisiting the Structure of Mesoporous α-d-Polysaccharide Gels. CHEMSUSCHEM. pp. 280-288. ISSN 1864-5631

https://doi.org/10.1002/cssc.201501354

ChemPubSoc Europe

DOI: 10.1002/cssc.201501354

CHEMSUSCHEM Full Papers

An Interesting Class of Porous Polymer—Revisiting the Structure of Mesoporous α-D-Polysaccharide Gels

Robin J. White,*[a, b, c] Peter S. Shuttleworth,[d] Vitaliy L. Budarin,[a] Mario De Bruyn,[a] Anna Fischer,[e] and James H. Clark[a]

The processes involved in the transformation of non-porous, native polysaccharides to their highly porous equivalents introduce significant molecular complexity and are not yet fully understood. In this paper, we propose that distinct changes in polysaccharide local short-range ordering promotes and directs the formation of meso- and micro-pores, which are investigated here using N_2 sorption, FTIR, and solid-state ^{13}C NMR. It is found that an increase in the overall double helical amylose content, and their local association structures, are responsible for formation of the porous polysaccharide gel phase. An exciting consequence of this local ordering change is elegantly revealed using a ^{19}F NMR experiment, which identifies the stereochemistry-dependent diffusion of a fluorinated chiral probe molecule (1-phenyl-2,2,2-trifluoroethanol) from the meso- to the micro-pore region. This finding opens opportunities in the area of polysaccharide-based chiral stationary phases and asymmetric catalyst preparation.

Introduction

Regarding biomass valorization in the context of nanomaterials, polysaccharides can be considered as excellent precursors given their abundance, low cost, and inherent functionality.[1] There is also the added benefit of the innate chirality of the monomer, polymer, and associated supramolecular structures.[2] The latter are dynamic, creating multiple metastable states related to torsion/rotation around the glycosidic bond that leads to transformations, including single-to-double helical structural transitions.[2b] Access to these different forms offers ■■"leads to" changed to "offers" ok?■■ great versatility and variety in the resulting properties of polysaccharide-derived materials.[1,3]

In the context of porous-material preparation, generally the specific surface area (S_{BET}) of polysaccharides in their native, extracted form (e.g., starch granules) is $<10\ m^2 g^{-1}$, a consequence of densely-packed H-bonded polymers, reflective of biological function (e.g., compact energy storage).[4] Previously, sol-gel-type approaches demonstrated the ability to expand (i.e., open up) the native polysaccharide state to produce high surface area, meso/microporous polysaccharides, including xero-, cryo-, and aero-gels.[3c,5] These functional, low density, polysaccharide-derived, porous materials (denoted hereon as PPDMs) represent interesting alternatives to traditional inorganic gels and have already found application as supports for acid, base, and metal catalysts.[6,7] Other demonstrated applications include antibacterial materials,[6a] chromatographic stationary phases,[5c] and adhesives.[8] PPDMs can also be converted to porous carbonaceous materials (i.e., Starbons),[9] which have found application as separation media[10] in the recovery of precious metals and as catalyst supports.[11,12] Recently a detailed study on the Starbon carbonization process linked mesopore formation to pre-existing amylose nano-agglomerates, emphasizing the importance of control over structuration of the parent PPDM.[13]

In the context of chirality, polysaccharides have found application in chiral separation science, typically by supporting them on high surface area silica.[14] However, the manufacture of supported polysaccharides is relatively tedious and expensive. Therefore, the exploitation of polysaccharide in such an application has vast potential, but requires further development and characterization of the PPDM phase to enable production of high surface area, porous materials. Furthermore, opening or expansion of polysaccharide structures, would also

[a] Dr. R. J. White, Dr. V. L. Budarin, Dr. M. D. Bruyn, Prof. J. H. Clark
Green Chemistry Centre of Excellence
University of York
Department of Chemistry
Heslington, York, YO10 5DD (UK)
E-mail: robin.white@ise.fraunhofer.de

[b] Dr. R. J. White
FMF—Freiburger Materialforschungszentrum
Stefan-Meier-Straße 21, 79104 Freiburg (Germany)

[c] Dr. R. J. White
Sustainable Catalytic Materials Group
Hydrogen Technologies Division
Fraunhofer Institute for Solar Energy Systems ISE
Heidenhofstraße 2, 79110 Freiburg (Germany)

[d] Dr. P. S. Shuttleworth
Departamento de Física de Polímeros, Elastómeros y Aplicaciones Energéticas
Instituto de Ciencia y Tecnología de Polímeros
CSIC
c/Juan de la Cierva 3, 28006 Madrid (Spain)

[e] Prof. A. Fischer
Universität Freiburg
Institut für Anorganische und Analytische Chemie
Albertstraße 21, 79104 Freiburg (Germany)

Supporting Information for this article is available on the WWW under http://dx.doi.org/10.1002/cssc.201501354.

allow more efficient modification of the structure as consequence of improved hydroxyl group accessibility. Owing to the known chirality of polysaccharides (e.g., helices), these surface hydroxyl groups display a strongly pronounced chirality.[15] Hence, the preparation of PPDMs potentially makes the materials stand out against classical carbonaceous or inorganic porous materials.

Following from the pioneering work of Che and coworkers concerning the preparation of chiral templated inorganic materials,[16] recent reports demonstrated the exploitation of cellulose nanocrystals in the synthesis of free standing, chiral nematic (e.g., micro- and meso-porous) films.[2a] This process involves co-condensation of a liquid-crystalline cellulose nanocrystal phase with either silica (through a sol-gel process)[15] or supramolecular co-templating with urea/formaldehyde.[17] The observed photonic properties of the resulting materials, the result of "macro" chirality, was reflective of a lyotropic chiral nematic liquid phase of cellulose nanocrystrals with a left-handed helical structure.[18] Whilst nanoporous examples were produced in this manner, there are no reports that demonstrate chirality in the pore structuring at the small molecule size range (i.e., micro- or meso-pores), which will be necessary to infer application advantages (e.g., asymmetric catalysis).

The manipulation of polymer interactions in the preparation of new polysaccharide-based nanomaterials could lead to the production of structural mimics of naturally occurring nanostructures (e.g., produced in cell morphogenesis).[19] In this context, following from our previously reported work,[20] this article sheds new light on the physicochemical and textural characteristics of porous poly-α(1→4)-D-glucopyranoses, using exemplary materials based on high amylose corn starch and pure amylose. This understanding and description aims to enable subtle manipulation of porosity and surface properties of PPDMs, which is illustrated here by the diffusion of a chiral molecule probe in the porous polysaccharide network.

Results and Discussion

Regarding PPDM preparation, there are three key steps in material preparation, namely: **1**) gelatinization, **2**) recrystallization or retrogradation, and **3**) solvent exchange/drying. During step **1**, the polysaccharide (e.g., high amylose corn starch; denoted as HACS) is heated in water typically above a temperature defined as the gelatinization temperature.[21,22] Step **1** results in an endothermic disruption of polysaccharide ordering[23] in which ■■ok?■■ water acts to plasticize, penetrate, and disrupt the H-bonded network, solubilizing the polysaccharide and eventually melting any crystallites as the system temperature increases to produce a disordered/random coil polymer solution. In Step **2**, when the system is typically cooled (retrogradation), localized ordered polymer associations are established to produce an aqueous gel phase of predominantly amorphous character. ■■Changes to the previous sentence ok?■■ As the gel is not at thermodynamic equilibrium, the system attempts to reorganize and minimize surface energy, increasing the relative "local" ordering of the polysaccharides.

Taking native starch as an example, amylopectin is known to be the major crystalline component.[24] X-ray diffraction (XRD) studies indicated that the long-range order present in the starch granule is lost during gelatinization and not recovered during retrogradation, indicating gel network formation is the product of short-range inter- and intra-molecular interactions.[25] Therefore, steps **1** and **2** generate new localized semi-crystalline amylose-rich domains composed of aggregated polysaccharide (e.g., double) helices.[22,24,25] Step **3** is employed to reduce the high surface tension of pore-bound water and the collapse of the pore structure during drying, preserving the "expanded" PPDM gel structure (the origin of the porosity and high surface area)[20] into the cryo-, xero- or aero-gel equivalent.[1,3c,20]

In the following study, HACS is used as an exemplary precursor for PPDM xerogel preparation, with the product denoted as xero-MS (i.e., xerogel mesoporous starch). To demonstrate the reproducibility ■■repeatability changed to reproducibility ok?■■ of our optimized synthesis, an important consideration when working polymers of a biological origin, five replicate xero-MS samples were prepared and characterized using N_2 sorption (Table S1 ■■1S changed to S1. Correct?■■ in the Supporting Information). xero-MS samples presented a mean S_{BET} of 190 $m^2 g^{-1}$, with minimal variation observed between batches (standard deviation (SD) of ± 2 $m^2 g^{-1}$). Pore volumes were large ($V_{total} > 0.7$ $cm^3 g^{-1}$), of which mesoporosity accounted for $>80\%$ (~0.60 $cm^3 g^{-1}$), again with good reproducibility ■■Here again. Ok?■■ ($SD_{mesopore} = \pm 0.02$ $cm^3 g^{-1}$). A mean average pore diameter (APD) of 9.5 nm was calculated, although a degree of variation between batches was observed for this textural parameter, attributed to the metastable nature of the aqueous polysaccharide gel.

The transformation of non-porous HACS (Figure 1 A) to the high surface area, predominantly mesoporous xero-MS is clearly observed using SEM, revealing a highly textured, interconnected porosity (Figure 1 B–C). Material morphology was found to be somewhat variable throughout the product at the >1 μm scale, potentially the result of collapsed granule structures induced by polysaccharide solubilization during the gelatinization process. Gel formation leads to a consistent, uniform, material texture at the sub-200 nm level, composed of interconnected mesopores and small diameter macropores (Figure 1 C).[10,20] N_2 sorption analysis generated Type IV isotherms, characteristic of a mesoporous material with the associated pore size distribution presenting a bimodal profile (i.e., contribution from both micro- and meso-pores; Figure 1 D).[26] The absence of a pronounced plateau region in the sorption isotherm as relative pressure approaches unity reflects a pore structure composed of slit-shaped and intra-particulate mesoporosity.[27]

Concerning the description of local polysaccharide ordering in xero-MS, qualitative information can be derived from FTIR spectroscopy (Figure 2).[28] Both the parent HACS and xero-MS present similar generic bands in four key spectral regions: <800 cm^{-1} (the anomeric region), 1500–800 cm^{-1} (the "fingerprint" pyranose region), 3000–2800 cm^{-1} (ν(C–H) deformation region), and 3600–3000 cm^{-1} (ν(O–H) stretch region)

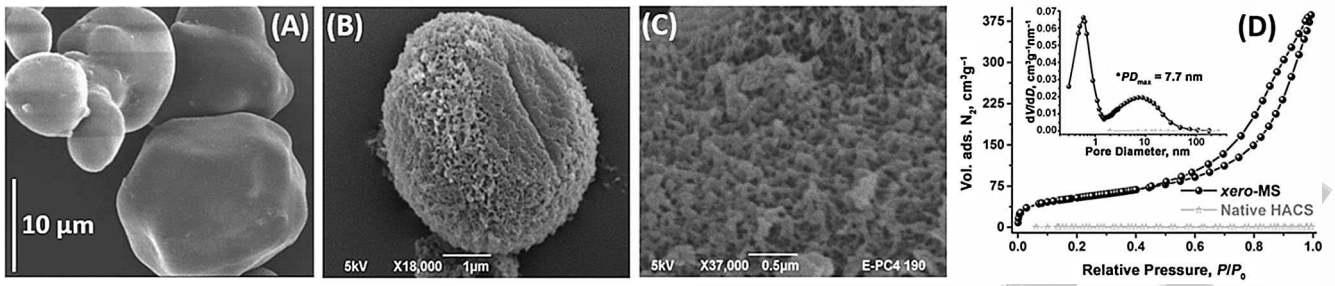

Figure 1. Scanning electron microscopy images of (A) native high amylose corn starch (HACS), (B–C) xerogels prepared from HACS denoted as xero-MS, and (D) N_2 sorption isotherms and corresponding Barrett–Joyner–Halenda (BJH) pore-size distributions (inset) for HACS and xero-MS.

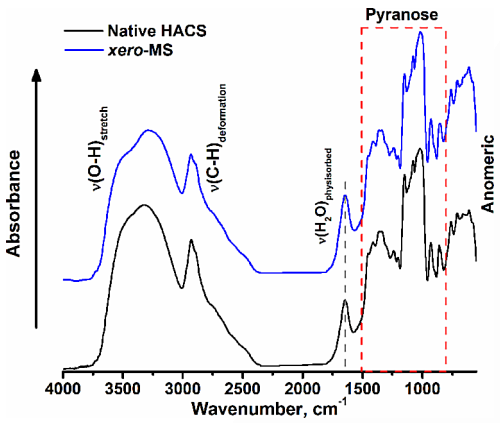

Figure 2. FTIR (diffuse reflectance infrared spectroscopy, DRIFT) spectra depicting the four main band regions of native and xerogel (xero-MS) forms of high amylose corn starch (HACS).

(Table 2S).[28] A band at 1642 cm^{-1} is attributed to the deformation vibrations of the O–H bond from strongly bound water molecules. As might be expected, both HACS and xero-MS present complex modes at wavenumbers <800 cm^{-1}, a product of glucose ring skeletal vibrations. Poorly resolved bands at 860, 761, 708, 610, and 574 cm^{-1} are observed in both spectra, with bands at 708 and 610 cm^{-1} being more intensely resolved for xero-MS, suggesting a network transformation. This is proposed to be related to the orientation/conformation of the glucose (or maltose) repeat units and/or the H-bonding network. This is reflected further by changes in the ν(O–H) stretching and ν(C–H) deformation modes. The maxima in the 3600–3000 cm^{-1} region shift from a broad band centered at 3322 cm^{-1} for HACS to a more resolved band centered at 3288 cm^{-1}, with a secondary band present as a shoulder at 3487 cm^{-1}, for xero-MS. Bands in this region are known to be sensitive to the polysaccharide network H-bonding,[28] and in this context reflect amylose reorganization (e.g., through a coil to helix transition) during recrystallization. Alteration in the relative peak intensities in the 3000–2800 cm^{-1} region (i.e., $-CH_2$ deformation modes) are also observed for xero-MS (relative to non-porous HACS), suggesting a re-ordering and re-association of C-6 hydroxyls during the formation of xero-MS phase.

Previous reports demonstrate the use of FTIR spectroscopy in polysaccharide conformation investigations particularly regarding starch processing (e.g., gelatinization and recrystallization).[29,30] In this context, FTIR spectroscopy is particularly sensitive to the key vibrations (e.g., ν(C–O), ν(C–H), and ν(O–H)). This means analysis of the local bonding environment and short-range ordering of starch polysaccharides is possible. This cannot be otherwise observed in these complex "amorphous" polymeric systems for example by powder XRD. In this context, bands at 1047 and 1022 cm^{-1} are well known to reflect the ordered and amorphous components of starch respectively. It is also known that the peak area ratio of the absorbance at 1047/1022 cm^{-1} provide a relative measure of the degree of polysaccharide ordering[20,31] (denoted hereon as the local ordering ratio, LOR). In terms of processing, retrogradation is known to increase the LOR, reflective of the transition from an initially amorphous gel to a relatively more ordered polysaccharide gel (and ultimately phase separation).[20]

A range of xero-MS samples prepared under a variety of conditions (Table S3; i.e., during the optimization of our PPDM preparation procedure) were analyzed using this FTIR approach (Figure 3 A–D). Each sample presented a different S_{BET} and porous expansion (Table S4). The 1500–800 cm^{-1} region (i.e., the pyranose fingerprint) was found to be particularly sensitive to the transition from the non-porous to porous state. Sharpening and enhanced resolution of bands in the 1200–960 cm^{-1} region were observed with increasing porosity (i.e., S_{BET} and mesopore volume, V_{meso}) ■■Definition added. Ok?■■. Therefore, the aforementioned LOR (i.e., $A_{1047\ cm^{-1}}/A_{1022\ cm^{-1}}$) was calculated as the change relative to the value for non-porous, ungelatinized HACS. Based on our and other previously reported methods, Gaussian peak fitting of the respective extracted FTIR spectra of xero-MS samples was performed using previously reported band assignments,[28–,31] using a six peak protocol with fixed positions at 1022 and 1047 cm^{-1}, generating data sets with good correlation factors (i.e., $R^2>0.996$). Plots of LOR versus S_{BET} and V_{meso} present 1st order exponential relationships (Figure 3 E–F). These relationships are presumably associated with the relative transition from amorphous to more locally ordered H-bonded networks in the gel phase, which is composed of polysaccharide double helices. Calculation of S_{BET} and V_{meso} maxima from the first-order exponential equation generated values of 184($\pm$9) $m^2 g^{-1}$ and 0.60($\pm$0.04) $cm^3 g^{-1}$ respectively, agreeing well with the aforementioned experimental values prepared using the optimized preparation route (Table S1).

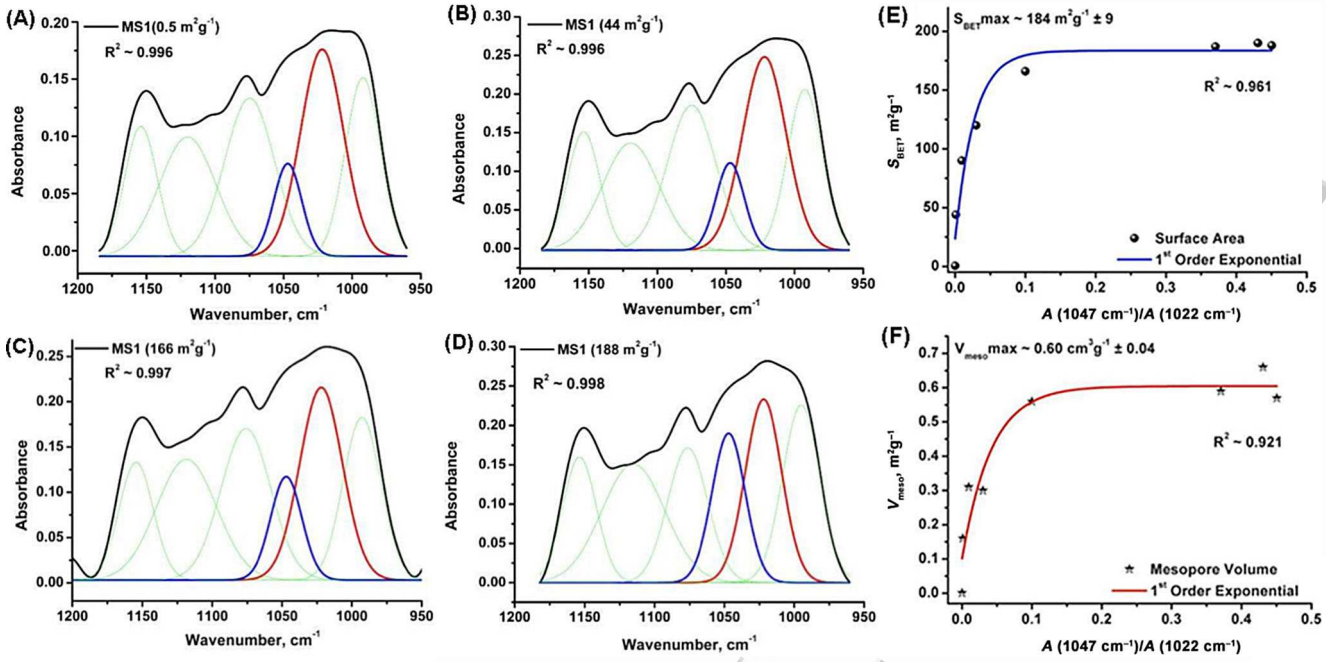

Figure 3. Extracted DRIFT spectra (and corresponding Gaussian fixed-peak deconvolutions) in the 1200–950 cm^{-1} region for xero-MS presenting different surface areas: (A) 0.5, (B) 44, (C) 166, and (D) 188 m^2g^{-1}; relationship between polymer ordering ratio $A_{1047\ cm^{-1}}/A_{1022\ cm^{-1}}$ and textural properties for xero-MS: (A) surface area (S_{BET}) and (B) mesopore volume (V_{meso}).

The increase in the LOR is presumed reflective of increasing double helical content in the expanded material, derived form a transition from the free coil phase (after gelatinization) to the double helical form (after retrogradation) of the amylose component. Such intermolecular processes are well known to lead to 3D hydrate gel structures in polysaccharide (e.g., amylose) gels,[32,33] whereas computational modelling of amylose indicates that an amylose double helix is thermodynamically preferred (i.e., vs. a single helix).[32,33] The correlation between the LOR and textural properties may therefore be related to localized ordered amylose-rich structures, resulting in the observed phase separation during gel preparation and formation of the xero-MS phase.

Complimentary to this FTIR analysis, it is known that the multiplicity of the C-1 resonance in solid-state ^{13}C NMR provides information regarding crystallinity and conformation in polysaccharides (e.g., single vs. double helices).[34] For example, the multiplicity of the C-1 resonance is known to be related to polymer packing in the starch granule.[34] Therefore, ^{13}C cross polarization magic angle spinning (CP-MAS) ■■Definition added here. Ok?■■ NMR spectra for both HACS and xero-MS were acquired (Figure 4). To demonstrate the importance of amylose in the formation of the high surface area/mesoporous structures (as postulated previously[20]), amylose and an amylose xerogel (denoted as xero-amylose) were also analyzed. The ^{13}C CPMAS NMR spectra for non-porous HACS and xero-MS presented resonances typical for HACS.[35] Examination of the spectral fine structure and intensity of the respective resonances indicated a number of significant differences between the non-porous and xerogel forms of both HACS and amylose. For HACS, characteristic resonances are observed at $\delta = 103.2$, 100.9, and 100.1 ppm The resonance at $\delta = 103.2$ and 102.8 ppm relates to the single helix conformation of amylose (i.e., a V-type or amorphous phase).[34–36] In accordance with the literature, resonances at $\delta = 100.9$ and 100.1 ppm reflect double helical polysaccharide packing.[34–36] Based on a comparison of Figure 5A and B with C and D, it can be seen that gelation reduces the amorphous or V-type content in favor of the local ordered packing of double polysaccharide helices, as exemplified further in Figure 5E and F.

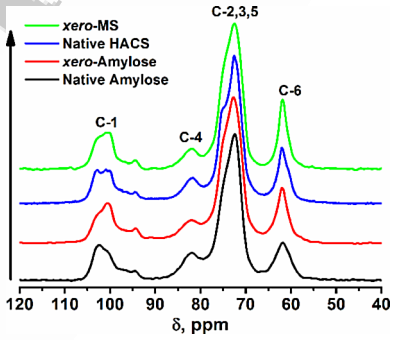

Figure 4. ^{13}C CP-MAS NMR spectra of the native and xerogel (xero-MS) forms of high amylose corn starch (HACS) and pure amylose.

The resonance at $\delta = 103$ ppm is well known to be associated with a single amylose helix conformation (often referred to as V-type amylose).[35,36] For xero-MS, this resonance is reduced in relative intensity and resolution, being broader and amorphous in shape, whereas resonances at $\delta = 101.0$ and 99.9 ppm resolve as a doublet, proposed to reflect the increase in relative double amylose helices (i.e., B-type hexagonal amy-

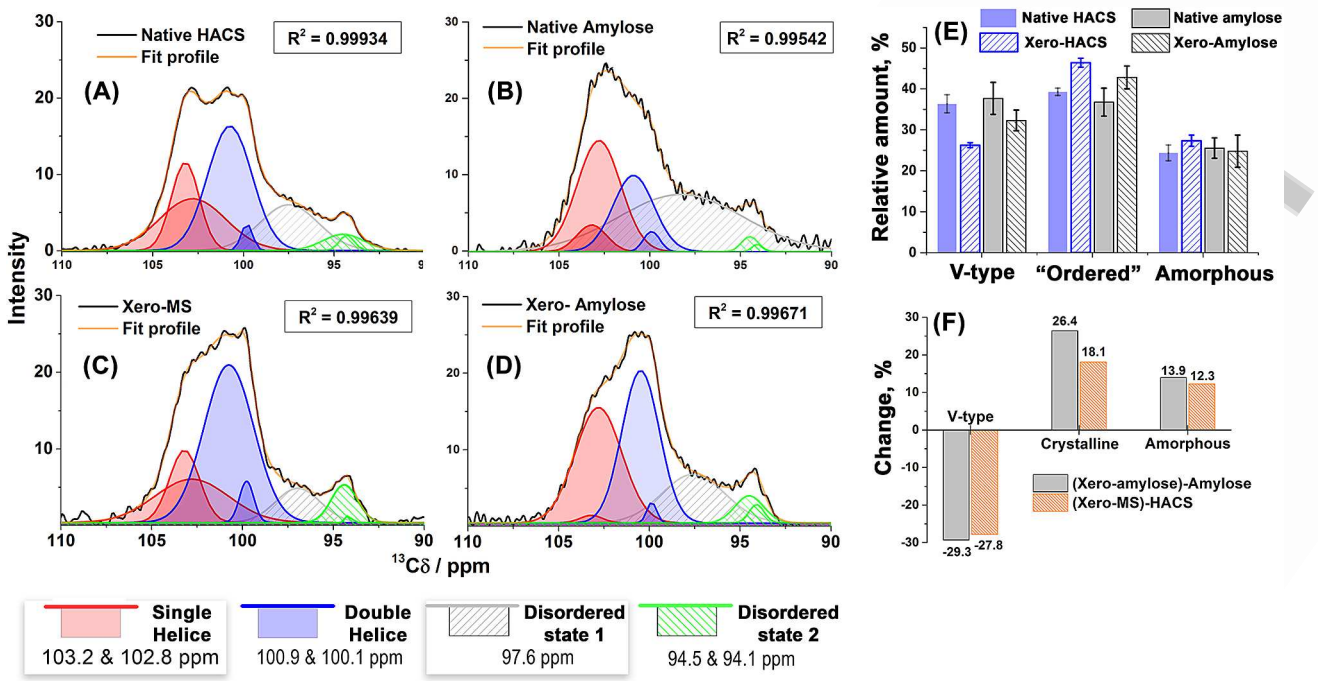

Figure 5. Extracted and deconvoluted ^{13}C CP-MAS NMR spectra in the region of $\delta = 110$–90 ppm for (A) native HACS ($S_{BET} < 5\ m^2 g^{-1}$), (B) native amylose ($S_{BET} < 10\ m^2 g^{-1}$), (C) xero-MS ($S_{BET} > 180\ m^2 g^{-1}$), and (D) xero-amylose ($S_{BET} > 180\ m^2 g^{-1}$); (E) The relative amount of V-type, ordered, and amorphous components of the respective polysaccharides; and (F) the relative change of the same components (as derived from the corresponding peak areas in A–D).

lose packing).[35,36] The resonance at approximately $\delta = 94$ ppm is known to reflect constrained linkages in a poorly favored conformational state (e.g., the metastable porous xerogel state).[34–36] Both xero-MS and xero-amylose show a relative increase in the resolution of this resonance, presumed to be the result of an increased contribution to the overall material state from energetically unfavorable conformation(s). The reduced relative intensity and resolution of the resonance at $\delta =$ 74.9 ppm in the xerogels corresponds with a broadening of the C-2, -3, and -5 resonances, and the formation of a comparatively less ordered system.[34–36] The intensity of the $\delta =$ 62.2 ppm resonance, relative to the broad intense resonance at $\delta = 72.5$ ppm, also increases for xero-MS; again proposed to be reflective of less favorable, locally ordered H-bonded networks.

To aid this discussion, deconvolution of the ^{13}C CPMAS NMR spectra in the region $\delta = 120$–90 ppm was performed for HACS, amylose, xero-MS, and xero-amylose (Figure 5). Deconvoluted spectral peaks associated with the resonance at $\delta =$ 102.9 ppm (i.e., single helices) are reduced in their relative contribution to the overall xerogel structure (Figure 5 E–F). Based on this information, it is proposed that single helix amylose recrystallizes after gelatinization and retrogradation to form double helices. This analysis reveals that this occurs in both xero-MS and xero-amylose, with a greater contribution to deconvoluted peaks associated with resonances in the $\delta = 101.5$–98 ppm range. It is important to note that in HACS, an inherent contribution to double helical content exists as a consequence of the presence of amylopectin. This agrees well with the discussed FTIR data, demonstrating a weakening of the H-bonding intensity, the result of the high surface area, porous phase formation (Figure 2).

The production of such PPDMs is very interesting from a green chemistry perspective, but it also has the potential to allow production of materials with unique pore structuring (i.e., based on helical structures). For example, the double helix of amylose is known to have a left-handed orientation.[33] Therefore, if it can be shown that the material porosity presents chiral domains; this could open further interest in PPDMs (e.g., asymmetric catalysis, chiral chromatography, etc.). However, the characterization of chiral porosity represents somewhat of challenge at the nanoscale. In this context, Tavener and coworkers examined the behavior of physisorbed, fluorinated reporter probe molecules using MAS NMR, utilizing the obtained results to describe and characterize the surface properties of a range of high surface area, porous solids.[37] Using reporter molecules with different bonding characteristics, they were able to separate the effects of specific chemical interactions from non-specific electrostatic bonding characteristics with the material surface, with the chemical shift of the ^{19}F nucleus being very sensitive to both chemical structure and physical state or environment of the probe molecule.

Inspired by this approach, the enantiomers of 1-phenyl-2,2,2-trifluoroethanol were employed as chiral reporter molecules to identify any chiral dependent behavior based on the ^{19}F chemical shift for each enantiomer in the physisorbed state. In this experiment, xero-MS was probed with the given enantiomer (loading: 0.03 micromoles per unit surface area, $\mu mol\ m^{-2}$) and the corresponding ^{19}F MAS NMR spectra acquired. Interestingly, two ^{19}F chemical shifts were observed for

the *R* enantiomer at $\delta = -76.4$ and -73.2 ppm (Figure 6A). This was at first surprising as identical experiments performed using a comparative, high surface area, predominantly mesoporous K60 silica gel generated a spectrum featuring only one single ^{19}F resonance (Figure S1), whereas liquid phase spectra present only a single resonance at $\delta = -78.9$ ppm.[38] Furthermore, after spectra acquisition at extended experiment times, the relative intensities of these two resonances presented time dependent behavior (Figure 6A). The resonance at $\delta = -76.4$ ppm was observed to reduce in intensity relative to $\delta = -73.0$ ppm as a function of the experiment time, potentially describing the diffusion of the probe molecule from one physisorption site to another. The experiment was repeated using the *S* enantiomer under identical conditions. Physisorption of the *S* enantiomer on xero-MS also generated two ^{19}F resonances but with marginally different chemical shifts at $\delta = -76.2$ and -73.5 ppm for the more and less intense resonances, respectively. A change in relative peak intensities between the two resonances was also observed with respect to time for the *S* enantiomer. Therefore, ^{19}F NMR spectra acquisition was repeated for both enantiomers and acquired at three hourly intervals over a 21 h experimental period (Figure 6A; $t = 0$, 6, and 21 h).

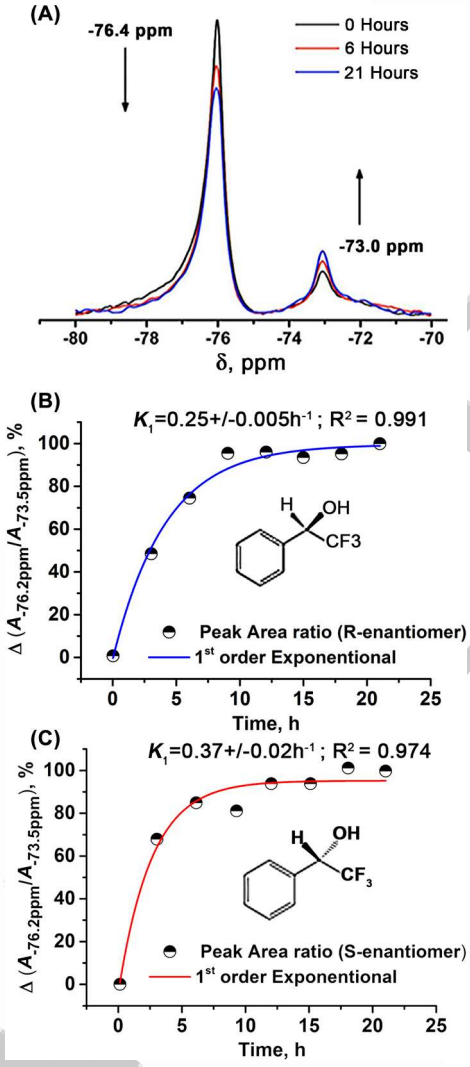

Figure 6. (A) ^{19}F MAS NMR spectra of physisorbed (*R*)-(−)-1-phenyl-2,2,2-trifluoroethanol on xero-MS acquired at different time intervals; 1st order kinetic analysis of the rate of diffusion of the enantiomers (B) (*R*)-(−)-1-phenyl-2,2,2-trifluoroethanol, and (C) (*S*)-(+)-1-phenyl-2,2,2-trifluoroethanol.

Review of the collected data and subsequent calculation of the respective resonance peak areas for each spectrum allowed calculation of the area ratio of the two peaks and the percentage change relative to the spectra acquired at $t = 0$ h. A first principles kinetic analysis of this data based on a first-order exponential equation, generated a first-order rate constant of 0.25 h^{-1} and 0.37 h^{-1} for the *R* and *S* enantiomers respectively (Figure 6B–C). Importantly the observed kinetic behavior was found to be reproducible and repeatable on two different NMR machines. It is postulated that the differences in the kinetic analysis, described here as the rate of enantiomer migration or diffusion from the lower to higher chemical shift sites, is potentially a product of a stereochemistry-limited diffusion step from a surface (or mesopore) site to a micropore site (e.g., the internal, hydrophobic cavity of the left-handed amylose double helix). In this context, Shimada et al. previously calculated that an amylose double helix has a cavity or entrance diameter in the range of 0.60–1.04 nm[33a] such that this cavity can be thought of as a continuous polymeric form of a cyclodextrin, the nature of which will be hydrophobic and likely to accommodate or trap substituted aromatic compounds of the type used in this NMR probing experiment.[39] This is a very interesting finding and represents a rather unique porous material feature, which through further research could become exploitable in applications, such as selective extraction, separation, or asymmetric catalysis. The description of the PPDM xerogels in this manner also raises the question of whether this chiral pore structuring can be successfully maintained during the preparation of carbonaceous-derivatives (i.e., in Starbons manufacturing process), opening further applications and biomass valorization opportunities.

Conclusions

The preparation of porous starch-derived polymer xerogels (e.g., xero-MS) with specific surface areas > 180 $m^2 g^{-1}$, large mesoporous domains and volumes (> 0.6 $cm^3 g^{-1}$), and the formation of an expanded phase, were shown to be the consequence of local, short range ordering behavior of amylose. Based on a combined FTIR and NMR approach, coupled with the synthesis of a pure amylose xerogel, characterization of the local polymer ordering was revealed, demonstrating the transition from a predominantly random polymer coil-based phase in the original (non-porous) polysaccharide to a relatively double helical amylose-rich phase. Based on an innovative ^{19}F NMR reporter molecule experiment, the inherently helical porous system of xero-MS was revealed to possess a chiral, stereochemistry-dependent diffusion character, proposed to be based on micropore entrances created through an increase in the content of amylose double helices within the porous gel structure. The presented results demonstrate the unique nature of porous polysaccharide-derived materials, here exem-

plified by an amylose-based system, featuring a highly mesoporous, chiral pore system, offering vast potential for a number of high value applications (e.g., asymmetric catalysis and chiral separation science).

Experimental Section

Materials and methods

Purified high amylose corn starch (HACS) was purchased from National Starch Food Innovation Plc. (Manchester, UK) and used as received. Pure amylose was purchased from Sigma–Aldrich (≥99% purity) and was used as received. All solvents used were purchased from Fischer Scientific at reagent grade purity and used without further purification. ^{19}F NMR reporter molecules (i.e., (*S*)- and (*R*)-(−)-1-phenyl-2,2,2-trifluoroethanol) were purchased from Sigma–Aldrich (≥99.0% purity) and were used as received.

Preparation of xero-MS from HACS

HACS and deionized water (at a mass ratio of 1:20) were stirred at 700 rpm for 10 min in a modified household pressure cooker prior to heating (volume = 3 L, operating conditions 120 °C/80 kPa). The lid component of the device was modified with an aluminium enclosure facilitating the insertion of a thermocouple. The system was heated to 120 °C (30 min) followed by an isothermal period of 45 min. Upon returning to atmospheric pressure, the lid was removed, and the resulting solution decanted into powder drying jars. The vessels were then sealed and the gels retrograded (at 5 °C/48 h). The resulting gel was then solvent exchanged and dried. The full experimental procedure is detailed in the Supporting Information. The preparation of an amylose-based xerogel (denoted as xero-amylose) was conducted as for xero-MS, however at the 1.0 g precursor scale.

Characterization

N_2 sorption analysis

Porosimetry analysis was performed using a Micromeritics ASAP 2010. Samples were degassed at 60 °C under vacuum (< 10^{-2} Pa) on the apparatus for at least 3 h prior to analysis. Data processing was performed using ASAP 2010 version 5.02 and OriginPro (v9.1) software. N_2 sorption isotherms were measured at −196 °C. Specific surface areas (S_{BET}) were determined using the Brunauer–Emmett–Teller (BET) ■■Definition added. Ok?■■ method, based on a N_2 cross-sectional area of 0.162 nm^2, calculated using a 10–20 point BET plot over a relative pressure range of (P/P_0) of 0.06–0.30, where a linear relationship was obtained.[40] Pore size distributions and mesopore volumes were calculated using the Barrett–Joyner–Halenda (BJH) ■■Definition added. Ok?■■ method and nitrogen adsorption data.[41] Dubinin–Radushkevich and *t*-plot analysis approaches were used in the determination of micropore volumes.[42]

Scanning electron microscopy

Scanning electron microscopy (SEM) images were recorded on a JEOL JSM-6490 LV (JEOL, Japan). Samples were mounted onto alumina sample holders with double sided reversible conductive carbon tape. Mounted material was Au/Pd coated on a high resolution sputter SC-7640 coating device at a sputtering rate of 1500 V min^{-1}, up to a thickness of 7 nm.

Diffuse reflectance infrared spectroscopy

Diffuse reflectance infrared spectroscopy (DRIFT) spectra were recorded using a Bruker Equinox 55 instrument equipped with a liquid N_2 cooled MCT detector. Resolution was 2 cm^{-1} and 1024 scans were averaged to obtain the spectra in the 4000–600 cm^{-1} range. Spectra were recorded using KBr as a reference. The samples were prepared by mechanically grinding all reactants to a fine powder [sample/KBr = 1:1000 (*w*/*w*)]. Subtraction of atmospheric CO_2 and H_2O from the resulting spectra was performed using the Bruker Opus software (v.5.5). Spectral peaks in the region of 1180–950 cm^{-1} were deconvoluted using a Gaussian-fitting model to reveal changes in the ratio between peaks at 1047 and 1022 cm^{-1}. Gaussian spectral deconvolution provided good fittings for all spectra ($R^2 > 0.995$). Peak assignments were based on positions from deconvolutions of starch in the dry state, as some peak resolution in the 1180–950 cm^{-1} region was lost owing to overlap with strong water absorption bands (i.e., 1004 cm^{-1}). Spectra processing was performed using the Bruker Opus v.5.5 software. Spectral peak fittings were performed using the OriginPro (v9.1) software and a 6-peak Gaussian fitting procedure using fixed peak positions at 1022 and 1047 cm^{-1} to define the local amorphous/crystalline or ordering ratio as reported previously.[20,29]

Solid-state ^{13}C CP-MAS NMR spectroscopy

^{13}C CP-MAS NMR spectra were obtained using a Varian VNMRS spectrometer operating at 100.56 MHz for ^{13}C. Referencing for all spectra presented was made with respect to tetramethylsilane at ambient temperature. Analysis of native HACS and xero-MS was performed under standard ^{13}C CP-MAS spectral acquisition using a ^{1}H $\pi/2$ pulse of 40.0 μs length and 1.0 s recycle, at a spin rate 5 kHz. A 4.0 mm zirconia rotor was used. Owing to the low sample density of xero-MS, the signal to noise ratio was particularly low. To counteract this, spectral acquisition was performed in the dipolar dephasing mode with a dephasing delay of 0.0 μs, amounting to a rotor-synchronized refocusing pulse on the carbon channel. This resulted in the removal of very broad signals arising from non-spinning carbon. The four acquired spectra were processed using OriginPro (v9.1) software, with data was extracted from the $\delta = 110$–90 ppm range, followed by a fixed 7-peak Gaussian deconvolution protocol based on the equation $[y = y_0 + (A/(w\sqrt{Pl}/2))e^{(-2((x-xc)^2/w)}]$, where $R^2 > 0.995$.

^{19}F MAS NMR probing experiment

The following method was adapted from a previously reported ^{19}F NMR method developed at the Green Chemistry Centre of Excellence.[20] xero-MS was thoroughly dried under vacuum at 60 °C on a Schlenk line for 1 min, 8 h prior to analysis. Samples were prepared by mixing accurately-weighed masses of the dried material and reporter molecule (e.g., (*R*)-(−)-1-phenyl-2,2,2-trifluoroethanol; 0.03 μmol m^{-2}), which were immediately sealed in a screw-top vial and left to equilibrate for approximately 1 h before analysis. Standard ^{19}F NMR spectra were obtained under MAS conditions on a Bruker Avance 400 spectrometer operating at 376.499 MHz in a 4 mm zirconia rotor. A single-nucleus, one-pulse acquisition method was used, with a recycle delay of 10 s. Typically 64 transients were collected at a spin rate of 10 kHz. Chemical shifts were

calibrated using liquid C_6F_6 as a reference at −163.0 ppm (relative to $CFCl_3$ at 0 ppm). For each transient, 4096 data points were acquired using a $\pi/2$ pulse of 3.5 μs, receiver bandwidth of 90 kHz, and a recycle delay of 10 s. Spectra were collected every 3 h over an experimental window of 21 h. Repeat experiments were performed under the same experimental conditions at the EPSRC Solid State NMR service, University of Durham, UK, using a Varian Unity Inova system operating at 282.09 MHz for ^{19}F, producing practically identical data sets. The acquired spectra were processed using Origin (v9.1) software and a Gaussian 2-peak deconvolution protocol where $R^2 > 0.996$. Experiments were also performed using amorphous K60 silica for comparison.

Acknowledgements

The authors would like to thank the members of the Green Chemistry Centre of Excellence for their input and useful discussions. We are particularly grateful to Dr. S. Tavener (University of York, UK) and Dr. D. C. Apperley (University of Durham, UK) for their fruitful discussions and assistance with all things regarding NMR. R.J.W. and J.H.C. would like to thank the Engineering and Physical Science Research Council (EPSRC), UK, for providing DTA funding. Thanks are given to Ms. M. Stark for her assistance with electron microscopy. Special thanks are also given to Dr. P. Aguiar for his time and fruitful discussions. P.S.S. gratefully acknowledges the Spanish Ministry Economy and Competitivity (MINECO) for a Ramón y Cajal fellowship (RYC-2014-16759) and a proyecto de I+D+I para jóvenes investigadores (MAT2014-59674-JIN). R.J.W. and A.F. are grateful to the Institut für Anorganische und Analytische Chemie and Freiburger Materialforschungszentrum (Universität Freiburg) for core facility support. R.J.W. is grateful to the Fraunhofer Society and the Fraunhofer Institute for Solar Energy Systems ISE for financial support through the Fraunhofer-Attract program.

Keywords: chiral · diffusion · polysaccharides · porosity · xerogels

[1] R. J. White, V. Budarin, R. Luque, J. H. Clark, D. J. Macquarrie, *Chem. Soc. Rev.* **2009**, *38*, 3401.

[2] a) J. A. Kelly, M. Giese, K. E. Shopsowitz, W. Y. Hamad, M. J. MacLachlan, *Acc. Chem. Res.* **2014**, *47*, 1088; b) L. Kong, C. Lee, S. H. Kim, G. R. Ziegler, *J. Phys. Chem. B* **2014**, *118*, 1775.

[3] a) R. V. F. Quignard, F. Di Renzo, *New J. Chem.* **2008**, *32*, 1300; b) F. Quignard, F. D. Renzo, E. Guibal, *Top. Curr. Chem.* **2010**, *294*, 165; c) R. J. White, N. Brun, V. L. Budarin, J. H. Clark, M. M. Titirici, *ChemSusChem* **2014**, *7*, 670.

[4] L. Juszczak, T. Fortuna, K. Wodnicka, *J. Food Eng.* **2002**, *54*, 103.

[5] a) X. Chang, D. Chen, X. Jiao, *Polymer* **2010**, *51*, 3801; b) X. Mi, W. Wang, J. Gao, Y. Long, F. Xing, X. Wang, F. Xu, X. You, S. Li, Y. Liu, *Poly. Adv. Technol.* **2012**, *23*, 38; c) V. L. Budarin, J. H. Clark, F. E. I. Deswarte, J. J. E. Hardy, A. J. Hunt, F. M. Kerton, *Chem. Commun.* **2005**, 2903.

[6] a) R. J. White, V. L. Budarin, J. W. B. Moir, J. H. Clark, *Int. J. Mol. Sci.* **2011**, *12*, 5782; b) A. Primo, F. Quignard, *Chem. Commun.* **2010**, *46*, 5593; c) F. Xu, C. Peng, H. Lu, *Prog. Chem.* **2008**, *20*, 273.

[7] V. L. Budarin, J. H. Clark, R. Luque, D. J. Macquarrie, R. J. White, *Green Chem.* **2008**, *10*, 382.

[8] P. S. Shuttleworth, J. H. Clark, R. Mantle, N. Stansfield, *Green Chem.* **2010**, *12*, 798.

[9] V. Budarin, J. H. Clark, J. J. E. Hardy, R. Luque, K. Milkowski, S. J. Tavener, A. J. Wilson, *Angew. Chem. Int. Ed.* **2006**, *45*, 3782; *Angew. Chem.* **2006**, *118*, 3866.

[10] a) A. Muñoz García, A. J. Hunt, V. L. Budarin, H. L. Parker, P. S. Shuttleworth, G. J. Ellis, J. H. Clark, *Green Chem.* **2015**, *17*, 2146; b) R. J. White, C. Antonio, V. L. Budarin, E. Bergström, J. Thomas-Oates, J. H. Clark, *Adv. Funct. Mater.* **2010**, *20*, 1834; c) H. L. Parker, A. J. Hunt, V. L. Budarin, P. S. Shuttleworth, K. L. Miller, J. H. Clark, *RSC Adv.* **2012**, *2*, 8992; d) H. L. Parker, V. L. Budarin, J. H. Clark, A. J. Hunt, *ACS Sustainable Chem. Eng.* **2013**, *1*, 1311; e) A. Borisova, M. De Bruyn, V. L. Budarin, P. S. Shuttleworth, J. R. Dodson, M. L. Segatto, J. H. Clark, *Macromol. Rapid Commun.* **2015**, *36*, 774.

[11] a) R. Luque, J. H. Clark, K. Yoshida, P. L. Gai, *Chem. Commun.* **2009**, 5305; b) R. Luque, J. H. Clark, *Catal. Commun.* **2010**, *11*, 928.

[12] a) V. Budarin, R. Luque, J. H. Clark, D. J. Macquarrie, *Chem. Commun.* **2007**, 634; b) R. Luque, V. Budarin, J. H. Clark, P. S. Shuttleworth, R. J. White, *Catal. Commun.* **2011**, *12*, 1471.

[13] P. S. Shuttleworth, V. Budarin, R. J. White, V. M. Gun'ko, R. Luque, J. H. Clark, *Chem. Eur. J.* **2013**, *19*, 9351.

[14] Y. Okamoto, T. Ikai, *Chem. Soc. Rev.* **2008**, *37*, 2593.

[15] K. E. Shopsowitz, W. Y. Hamad, M. J. MacLachlan, *Angew. Chem. Int. Ed.* **2011**, *50*, 10991; *Angew. Chem.* **2011**, *123*, 11183.

[16] a) H. Qiu, Y. Inoue, T. Jin, S. Che, *Angew. Chem. Int. Ed.* **2009**, *48*, 3069; *Angew. Chem.* **2009**, *121*, 3115; b) H. Qiu, S. Che, *Chem. Soc. Rev.* **2011**, *40*, 1259.

[17] M. Giese, L. K. Blusch, M. K. Khan, W. Y. Hamad, M. J. MacLachlan, *Angew. Chem. Int. Ed.* **2014**, *53*, 8880; *Angew. Chem.* **2014**, *126*, 9026.

[18] R. H. Marchessault, F. F. Morehead, N. M. Walter, *Nature* **1959**, *184*, 632.

[19] T. T. Teeri, H. Brumer, G. Daniel, P. Gatenholm, *Trends Biotechnol.* **2007**, *25*, 299.

[20] R. J. White, V. L. Budarin, J. H. Clark, *ChemSusChem* **2008**, *1*, 408.

[21] N. J. Atkin, R. M. Abeysekera, S. L. Cheng, A. W. Robards, *Carbohydr. Polym.* **1998**, *36*, 173.

[22] a) T. Vasanthan, R. S. Bhatty, *Cereal Chem.* **1996**, *73*, 199; b) K. S. Sandhu, N. Singh, *Food Chem.* **2007**, *101*, 1499.

[23] N. J. Atkin, R. M. Abeysekera, A. W. Robards, *Carbohydr. Polym.* **1998**, *36*, 193.

[24] J.-L. Putaux, A. Buleon, H. Chanzy, *Macromolecules* **2000**, *33*, 6416.

[25] a) C. J. A. M. Keetels, G. T. Oostergetel, T. v. Vliet, *Carbohydr. Polym.* **1996**, *30*, 61; b) A. Imberty, H. Chanzy, S. Perez, A. Buleon, V. Tran, *J. Mol. Biol.* **1988**, *201*, 365; c) L. Smeller, *Biochim. Biophys. Acta Protein Struct. Mol. Enzymol.* **2002**, *1595*, 11; d) J. L. Jane, K. S. Wong, A. E. McPherson, *Carbohydr. Res.* **1997**, *300*, 219.

[26] a) S. J. Gregg, K. S. W. Sing, *Adsorption, Surface Area and Porosity*, Academic Press, London, UK, **1982**; b) D. H. Everett, *Pure Appl. Chem.* **1972**, *31*, 577.

[27] a) W.-C. Li, A.-H. Lu, C. Weidenthaler, F. Schüth, *Chem. Mater.* **2004**, *16*, 5676; b) T. Sasaki, S. Nakano, S. Yamauchi, M. Watanabe, *Chem. Mater.* **1997**, *9*, 602.

[28] a) P. D. Vasko, J. Blackwell, J. L. Koenig, *Carbohydr. Res.* **1971**, *19*, 297; b) K. I. Shingel, *Carbohydr. Res.* **2002**, *337*, 1445; c) M. Sekkal, V. Dincq, P. Legrand, J. P. Huvenne, *J. Mol. Struct.* **1995**, *349*, 349; d) R. Kizil, J. Irudayaraj, K. Seetharaman, *J. Agric. Food Chem.* **2002**, *50*, 3912.

[29] a) A. L. M. Smits, F. C. Ruhnau, J. F. G. Vliegenthart, J. J. G. v. Soest, *Starch/Staerke* **1998**, *50*, 478; b) J. J. G. van Soest, H. Tournois, D. D. Wit, J. G. G. Vliegenthart, *Carbohydr. Res.* **1995**, *279*, 201; c) O. Sevenou, S. E. Hill, I. A. Farhat, J. R. Mitchell, *Int. J. Biol. Macromol.* **2002**, *31*, 79; d) I. Capron, P. Robert, P. Colonna, M. Brogly, V. Planchot, *Carbohydr. Polym.* **2007**, *68*, 249.

[30] R. H. Wilson, M. T. Kalichevsky, S. G. Ring, P. S. Belton, *Carbohydr. Res.* **1987**, *166*, 162.

[31] R. H. Wilson, P. S. Belton, *Carbohydr. Res.* **1988**, *180*, 339.

[32] P. Rubens, J. Snauwaert, K. Heremans, R. Stute, *Carbohydr. Polym.* **1999**, *39*, 231.

[33] a) J. Shimada, S. Handa, H. Kaneko, T. Takada, *Macromolecules* **1996**, *29*, 6408; b) Y. Takahashi, T. Kumano, S. Nishikawa, *Macromolecules* **2004**, *37*, 6827; c) O. Nimz, K. Gessler, I. Usón, G. M. Sheldrick, W. Saenger, *Carbohydr. Res.* **2004**, *339*, 1427; d) H. W. Tsui, N. H. L. Wang, E. I. Franses, *J. Phys. Chem. B* **2013**, *117*, 9203; e) D. W. Griffiths, M. L. Bender, *J. Am. Chem. Soc.* **1973**, *95*, 1679.

[34] a) M. J. Gidley, S. M. Bociek, *J. Am. Chem. Soc.* **1988**, *110*, 3820; b) K. R. Morgan, R. H. Furneaux, N. G. Larsen, *Carbohydr. Res.* **1995**, *276*, 387; c) A. Lopez-Rubio, B. M. Flanagan, E. P. Gilbert, M. J. Gidley, *Biopolymers* **2008**, *89*, 761; d) V. J. McBrierty, K. J. Packer, *Nuclear Magnetic Resonance*

in Solid Polymers, Cambridge Academic Press, Cambridge, UK, **1993**; e) N. Atichokudomchai, S. Varavinit, P. Chinachoti, *Carbohydr. Polym.* **2004**, *58*, 383; f) M. J. Gidley, S. M. Bociek, *J. Am. Chem. Soc.* **1985**, *107*, 7040; g) R. P. Veregin, C. A. Fyfe, R. H. Marchessault, M. G. Taylor, *Macromolecules* **1986**, *19*, 1030.

[35] a) H. Thérien-Aubin, F. Janvier, W. E. Baille, X. X. Zhu, R. H. Marchessault, *Carbohydr. Res.* **2007**, *342*, 1525; b) W. Błaszczaka, J. Fornal, S. Valverde, L. Garrido, *Carbohydr. Polym.* **2005**, *61*, 132.

[36] a) R. L. Shogren, A. R. Thompson, R. V. Greene, S. H. Gordon, G. Cote, *J. Appl. Polym. Sci.* **1991**, *42*, 2279; b) I. Tan, B. M. Flanagan, P. J. Halley, A. K. Whittaker, M. J. Gidley, *Biomacromolecules* **2007**, *8*, 885; c) W. C. Obiro, S. S. Ray, M. N. Emmambux, *Food Rev. Int.* **2012**, *28*, 412.

[37] a) V. L. Budarin, J. H. Clark, F. E. I. Deswarte, K. T. Mueller, S. J. Tavener, *Phys. Chem. Chem. Phys.* **2007**, *9*, 2274; b) V. L. Budarin, J. H. Clark, S. J. Tavener, *Chem. Commun.* **2004**, 524.

[38] H. Kawai, Z. Yuan, E. Tokunaga, N. Shibata, *Org. Biomol. Chem.* **2013**, *11*, 1446.

[39] E. M. Martin Del Valle, *Process Biochem.* **2004**, *39*, 1033.

[40] S. Brunauer, P. H. Emmett, E. Teller, *J. Am. Chem. Soc.* **1938**, *60*, 309.

[41] E. P. Barrett, L. G. Joyner, P. P. Halenda, *J. Am. Chem. Soc.* **1951**, *73*, 373.

[42] a) Y. K. Tovbin, *Langmuir* **1999**, *15*, 6107; b) V. K. Dobruskin, *Langmuir* **2003**, *19*, 2134.

Received: October 8, 2015
Revised: November 19, 2015
Published online on ■■ ■■, 0000

R. J. White, P. S. Shuttleworth, V. L. Budarin, M. D. Bruyn, A. Fischer, J. H. Clark*

■■ – ■■

An Interesting Class of Porous Polymer—Revisiting the Structure of Mesoporous α-D-Polysaccharide Gels

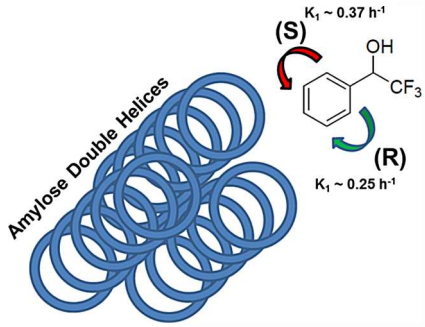

In a spin: A combined spectroscopic approach to the unravelling of the polysaccharide organization in mesoporous xerogels reveals a unique chiral diffusion character reflective of the assembly of amylose double helices. The results demonstrate the unique nature of porous polysaccharide-derived materials, exemplified by an amylose-based system, offering vast potential for a number of high value applications, such as asymmetric catalysis and chiral separation science.

White et al. demonstrate #chirality in #mesoporous #polysacchride #xerogels. SPACE RESERVED FOR IMAGE AND LINK

Share your work on social media! *ChemSusChem* has added Twitter as a means to promote your article. Twitter is an online microblogging service that enables its users to send and read text-based messages of up to 140 characters, known as "tweets". Please check the pre-written tweet in the galley proofs for accuracy. Should you or your institute have a Twitter account, please let us know the appropriate username (i.e., @accountname), and we will do our best to include this information in the tweet. This tweet will be posted to the journal's Twitter account @ChemSusChem (follow us!) upon online publication of your article, and we recommended you to repost ("retweet") it to alert other researchers about your publication.

Please check that the ORCID identifiers listed below are correct. We encourage all authors to provide an ORCID identifier for each coauthor. ORCID is a registry that provides researchers with a unique digital identifier. Some funding agencies recommend or even require the inclusion of ORCID IDs in all published articles, and authors should consult their funding agency guidelines for details. Registration is easy and free; for further information, see http://orcid.org/.

Dr. Robin J. White
Dr. Peter S. Shuttleworth
Dr. Vitaliy L. Budarin
Dr. Mario De Bruyn
Prof. Anna Fischer
Prof. James H. Clark